batteries

MDPI

Article

The Effects of Silicon Anode Thickness on the Electrochemical Performance of Li-Ion Batteries

Matea Raić [1,2], Krešimir Kvastek [3], Lara Mikac [1,2], Nikola Baran [4] and Mile Ivanda [1,2,*]

[1] Laboratory for Molecular Physics and Synthesis of New Materials, Ruder Bošković Institute, Bijenička c. 54, 10000 Zagreb, Croatia
[2] Research Unit New Functional Materials, Center of Excellence for Advanced Materials and Sensing Devices, Bijenička c. 54, 10000 Zagreb, Croatia
[3] Division for Marine and Environmental Research, Ruder Bošković Institute, Bijenička c. 54, 10000 Zagreb, Croatia
[4] Laboratory for Precipitation Processes, Division for Materials Chemistry, Ruder Bošković Institute, Bijenička c. 54, 10000 Zagreb, Croatia
* Correspondence: mile.ivanda@irb.hr; Tel.: +385-1-456-0928

Abstract: The electrode configuration is an important element in the development of Li-ion cells. The energy density is proportional to the loading of the active material. Therefore, increasing the electrode thickness is the simplest way to achieve higher capacities. In this paper, we compare the effects of three different thicknesses of Ag-decorated Si electrode anode (HCSi) on the electrochemical performances such as the SEI layer formation, impedances, and mass capacitances. We prepared three different silicon electrode thicknesses to optimize the electrodes: 20, 40 and 60 μm and measured in situ galvanostatic electrochemical impedance spectroscopy (GEIS). Using GEIS, we studied the intercalation mechanism of Li^+ ions in detail and found that despite having the same capacities (≈3500 mAh g^{-1}), the thinnest electrode, HCSi20, allows diffusion of Li^+ ions into the bulk, whereas thicker layers prevent smooth diffusion into the bulk of the silicon electrode due to increased layer resistance. The Voigt model was used to analyze the anomaly of the frequency dependence of the measured impedance, in which, the classical Randles circuit is connected in series with one or two R ‖ C parallel combinations. One R ‖ C circuit could be the result of the SEI formation, and the second R ‖ C circuit could be the contribution of Li. To increase the number of charge and discharge cycles, we improved the electrolyte by adding fluoroethylene carbonate (FEC), which reduced the capacity of the HCSi20 electrode to 50% of the initial capacity (≈3500 mAh g^{-1}) after 60 cycles, whereas it dropped to 20% of the initial capacity after 10 cycles without the addition of FEC.

Keywords: electrode optimization; anode thickness; galvanostatic EIS; electrolyte additive

check for updates

Citation: Raić, M.; Kvastek, K.; Mikac, L.; Baran, N.; Ivanda, M. The Effects of Silicon Anode Thickness on the Electrochemical Performance of Li-Ion Batteries. *Batteries* **2023**, *9*, 173. https://doi.org/10.3390/batteries9030173

Academic Editor: Jiangfeng Ni

Received: 22 February 2023
Revised: 9 March 2023
Accepted: 15 March 2023
Published: 17 March 2023

Copyright: © 2023 by the authors. Licensee MDPI, Basel, Switzerland. This article is an open access article distributed under the terms and conditions of the Creative Commons Attribution (CC BY) license (https://creativecommons.org/licenses/by/4.0/).

1. Introduction

Lithium-ion batteries (LiBs) are used as high-performance, portable, and rechargeable energy storage devices in a variety of applications. As the energy storage requirements continue to increase, graphite electrodes must be replaced to achieve higher capacities. Silicon, in this context, represents a new generation of anode materials. Its high theoretical capacity of 3590 mAh g^{-1} for $Li_{15}Si_4$ at room temperature is ten times higher than standard graphite. Since silicon is the second most common element in the Earth's crust, cost-effective mass production is not an issue [1]. However, the practical application of such electrodes is limited by volume expansion, which can be as much as 400% of the initial volume, causing stress and strain that causes electrode fracture and electrical insulation during cycling [2]. Currently, intensive research is underway to develop porous nanostructured silicon that can compensate for the volume expansion while also providing a large specific surface area for the diffusion of Li^+ ion [3,4]. When the electrode is first exposed to the electrolyte, a solid electrolyte interphase (SEI) form. Continuous volume changes lead to the reformation of the SEI layer and consumption of the electrolyte, as well as a fast capacity fade [5].

An important element in the development of Li-ion cells is the electrode configuration. The energy density is directly related to the loading of the active material. Therefore, to achieve higher capacities, the easiest way is to increase the electrode thickness [6].The critical electrode thickness where the energy density reaches its maximum varies depending on the electrode material and test conditions. Unlike laboratory-scale electrodes, which are ≈50 µm thick [7], conventional lithium-ion cell electrodes are 70 µm thick [8–10]. Most studies compare and optimize cathode thickness, including the work of Zheng et al. [11], which compares four NMC cathodes with different thicknesses (24 µm, 50 µm, 76 µm and 104 µm). The capacity retention after 500 cycles is 92% for the thinnest electrode, which is significantly higher than the 60% retention for the thickest electrode. Research shows that thicker electrodes achieve higher energy density but lower power density and faster capacitance decay [12].Thinner electrodes have better cycling performance due to lower charge transfer resistance along with better mechanical integrity. The increase in resistance is probably related to the formation of the SEI layer which consequently contributes to the total impedance of the cell. However, in most literature, anode thickness analyzes are based on graphite electrodes [13–16]. Since silicon anodes suffer from volume expansion upon cycling, it is very important to optimize the thickness. Thicker electrodes are favorable for the energy density increase, especially for low C rates. By raising the mass load of the active material, the proportion of inactive material, such as binder, separator, and current collectors, is decreased, improving cell energy and lowering costs. However, long transport pathways results in high ohmic resistances, so thick electrodes are unfavorable for Li^+ diffusion [12,17]. Although the internal resistance has been widely reported [11,18], few studies have considered the electrode thickness and diffusion through thicker electrodes.

In our previous work, we investigated a silicon honeycomb (HCSi) structure prepared by Magnesium Thermal Reduction (MRR) as a potential anode material for lithium-ion batteries previously reported [19]. For this purpose, a different content of silver nanoparticles (AgNP) was deposited on the HCSi structure to improve its conductivity. In summary, the HCSi sample, with the highest Ag content showed the lowest impedance and the highest intercalation intensity, resulting in an excellent specific capacity of 3333 mAh g^{-1} at 0.067 A g^{-1} [19]. In this research, we report a comparative study on the effects of three different HCSi anode thicknesses of the electrochemical performances such as the formation of SEI layer, impedances, and mass capacitances. The combined electrochemical techniques in different time domains can provide a deeper understanding of the mechanism of lithiation. As a result of Li^+ ion diffusion, the interphase Si/electrolyte becomes a complex interphase containing various types of resistive and capacitance elements, and electrochemical impedance spectroscopy appears to be an ideal technique for studying lithiation [16,20].

During the intercalation of Li^+, a series of polarizations occur. The Li ions from the electrolyte migrate to the silicon surface covered by the SEI, resulting in ohmic polarization (R_S). They diffuse through the SEI layer and produce an activation polarization corresponding to each step (R_{SEI}, R_{CT}). After Li_xSi_y alloying, the remaining Li^+ diffuse through the silicon and produce a concentration gradient, a concentration polarization [10]. As the electrode thickness increases, a higher concentration gradient is achieved [12]. Electrolyte additives can improve the composition and stability of a SEI by forming a thin SEI with low ionic resistance [21–23].

Each process step is a separate kinetic parameter that can be studied by electrochemical impedance spectroscopy (EIS) [24]. The overall process can be divided into separate steps based on frequency. Usually, impedance spectra are obtained by controlled-potential techniques (PEIS) after the system has reached a steady state [25]. Over 40% of the studies on the commercial Li-ion cells uses PEIS, typically with sinusoidal potential 5–10 mV. Commercial batteries, on the other hand, have much lower impedance than lab-scale cells, so a small changes in the input voltage can result in large output current [26]. For this reason, PEIS cannot determine the state of charge (SOC) and is therefore not suitable for investigation of Li-ion cells [27]. In this work, we measured in-situ EIS using galvanostatic electrochemical impedance spectroscopy (GEIS), in which a sinusoidal current is superimposed with a

fixed charge. The primary advantage of this technique is that the cell under test meets the stationarity conditions for valid impedance measurements.

Many studies have been performed by investigating the internal resistance of the electrode through charge transfer (R_{CT}) [11,18,28]. To fully explain the mechanism of the Li^+ ion diffusion, diffusion through the porous layer and the phase boundary between the electrode and electrolyte must be included [18]. We studied electrochemical processes in porous electrodes using in situ GEIS method, which include diffusion of Li^+ ion and charge transfer related to Li^+ intercalation.

These GEIS studies mainly focus on the impedance variation with different electrode thicknesses in the first cycle to study the kinetics and reaction mechanism of lithiation.

In addition, the poor cycling stability were investigated and improved by adding fluoroethylene carbonate (FEC) to the electrolyte. The basic idea behind electrolyte additives is that it has higher reduction potential than the solvent molecule, resulting in the formation of a stable SEI film and preventing decomposition of electrolyte which further leads to better performances of the lithium battery. Experimental and theoretical studies have recently demonstrated that FEC preferentially decomposes in contact with lithium, forming SEI film with the main component of small organic molecules and LiF. Increase of the LiF particles in the inorganic layer, in particular, can make the SEI film more dense, preventing further contact of lithium and electrolyte [29].

2. Experimental

2.1. Electrode Preparation

As the active material of the working electrode, previously described [19] Ag-decorated silicon (HCSi), was combined in a 60:20:20 ratio with carboxymethyl cellulose (CMC) as a binder and carbon black (CB) in H_2O as a solvent. Using a Doctroblade coating machine, the produced slurries were subsequently applied on an aluminum foil as a current collector. Electrode sheets were prepared in dry thicknesses of 20, 40 and 60 µm and dried at 60 °C for 12 h in vacuum. Round electrodes with a diameter of 18 mm were cut with an electrode punching tool. The samples were designated as HCSi20, HCSi40 and HCSi60, with an active material loading of ≈1.5 mg for HCSi20, ≈3 mg for HCSi40 and ≈4.5 mg for HCSi60.

2.2. Electrochemicall Cell Preparation

Figure 1 shows a "home-made" 2-electrode system used for electrochemical characterization assembled in argon-filled glove box (Mbraun, <0.1 ppm of H_2O and <0.1 ppm of O_2) using lithium foil as the counter electrode (CE) and glass fiber (18 × 1.55 mm) separator soaked with LP30 electrolyte (1M $LiPF_6$ in 1:1 dimethyl carbonate (DMC): ethylene carbonate (EC). Fluoroethylene carbonate (FEC), an electrolyte additive was added to the basic electrolyte at a concentration of 10% *v/v*. Working electrodes (WE) were Ag decorated Si nanostructure in different thicknesses (HCSi20, HCSi40, HCSi60).

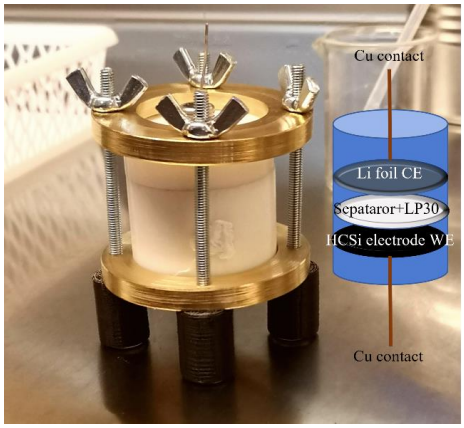

Figure 1. "Home-made" 2-electrode system for electrochemical measurements.

2.3. Instrumental Analysis

Field emission scanning electron microscope coupled with Energy-dispersive spectroscopy JSM 7000F (JEOL) was used to investigate the morphology of the obtained materials. Chronopotentiometric measurements and electrochemical impedance spectroscopy (EIS) measured by by Solartron FRA (Model 1250) with ECI (Model 1287) were used to determine the kinetics of lithiation and delithiation. EIS was performed in the frequency range from 100 kHz to 10 mHz with a current bias up to 10 µA. The cycle performance test was performed at 0.2 A g^{-1} current density.

3. Results

SEM images of the electrode cross-section after testing are shown in Figure 2. In a previous paper [19], the TEM microscope was used to determine the primary particle size of HCSi, which contains two types of NPs, larger (≈100 nm) and smaller (≈40 nm) particles with an active surface of 34.03 m^2 g^{-1}. According to the SEM, the electrode thickness is quite uniform since the electrodes are prepared in a controllable way. The aluminum foil has a thickness of about 6 µm. The observed changes in surface morphology in all three electrodes could be attributed to one of two degradation mechanisms: lithium metal deposition or oxidation in reaction with the electrolyte. The HCSi20 electrode has cracks that extend into the bulk, indicating good Li^+ diffusion in a thin film. Bulk changes and cracks are not observed for thicker electrodes, the majority of the lithium remains behind the active surface and does not diffuse into the bulk.

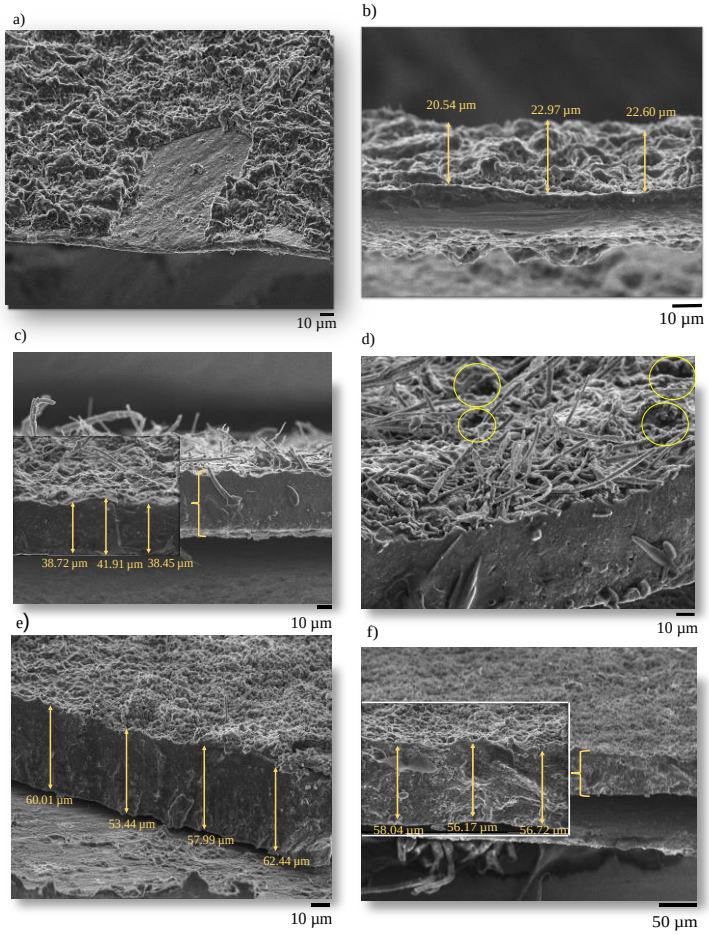

Figure 2. SEM images of the cross-sections of electrodes after testing: (**a**,**b**) HCSi20, (**c**,**d**) HCSi40, (**e**,**f**) HCSi60.

To confirm our assumptions, further SEM images of the samples HCSi20, HCSi40, and HCSi60 were obtained (see Figure 3). These images demonstrate the pulverization of the HCSi surface following lithiation (Figure 3a, before lithiation), especially in HCSi60. The interparticle porosity, which is obvious in Figure 3a, is not present in Figure 3b–d indicating pulverization. Moreover, Figure 3b supports lithiation into bulk.

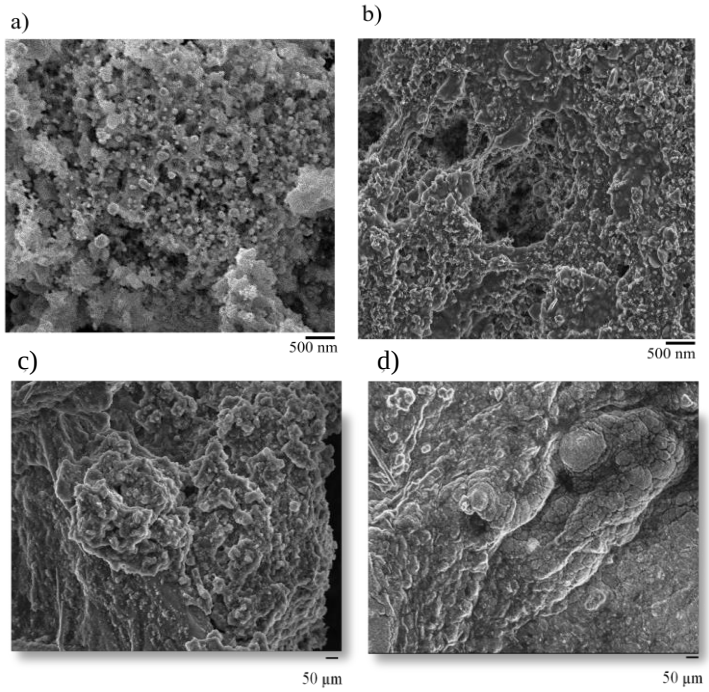

Figure 3. SEM images of (**a**) active material HCSi before testing, electrodes: (**b**) HCSi20, (**c**) HCSi40, (**d**) HCSi60 after testing.

Three different electrode thickness were studied as anode materials: HCSi20, HCSi40 and HCSi60. These electrodes were connected to the Li-electrode in a two-electrode cell and, after stabilization, were galvanostatically tested at a constant current of −100 µA.

Figure 4 shows the chronopotentiometric curves for the HCSi20, HCSi40 and HCSi60 electrodes with a constant current of −100 µA. After stabilization, the open circuit potential (OCP) of all three electrodes was ≈ +3.5 V. Above 1.2 V, the primary SEI forms, and below it, the process of Li^+ intercalation occurs, as seen in the chronopotentiometry curves for the electrode with the thinnest layer of active material, HCSi20. The dynamics of the potential change during the galvanostatic process, resulting in a change in the slope. Three potential regions with different Li^+ intercalation dynamics were observed, i.e., the formation of different forms of Li_xSi_y (shown in Figure 4, marked a, b, c) [30]. These regions were not observed in thicker layers, HCSi40 and HCSi60, implying that intercalation of Li^+ ion into the bulk is difficult, which may be related to the increase in resistance with increasing layer thickness.

The specific capacities of the electrodes were calculated using chronopotentiometry curves and are shown as inset in Figure 4. The specific capacities for all three electrode thicknesses are around 3500 mAh g^{-1}, but it is unknown whether some of the charge was used to generate an additional SEI rather than lithiation.

Figure 5a shows the galvanostatic charge and discharge for the HCSi20 electrode over ten cycles at current of 300 µA. Due to a higher current density, the capacity reaches 2400 mAh g^{-1} in the first cycle, which is lower than the chronopotentiometry discharge in Figure 4. The value of the initial capacity drops to 20% in the second cycle and remains constant for the next cycles.

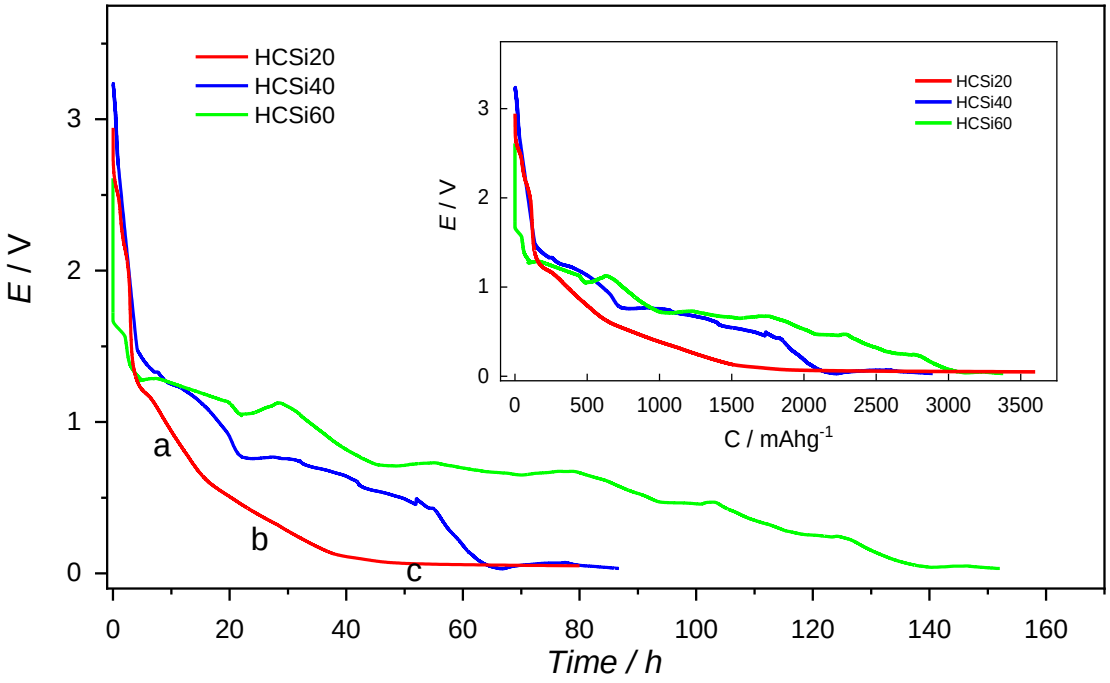

Figure 4. Chronopotentiometic curves for electrodes HCSi20, HCSi40 and HCSi60 at constant current of −100 µA. Galvanostatic discharge with specific capacities for electrodes HCSi20, HCSi40 and HCSi60 (inset).

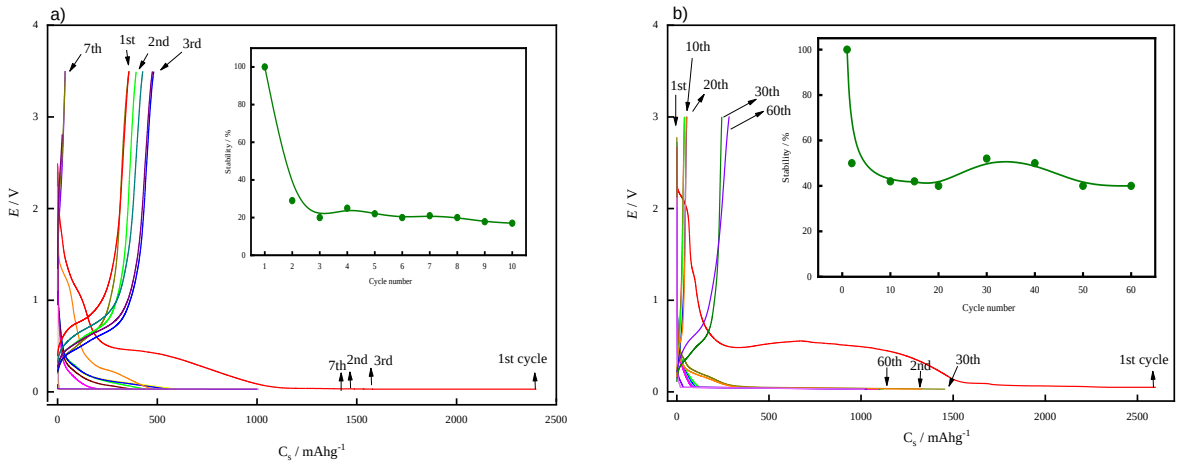

Figure 5. Galvanostatic charge / discharge at constant current 300 µA for: (**a**) HCSi20 electrode. Stability over 10 cycles (inset), (**b**) HCSi20 with FEC electrode. Stability over 60 cycles (inset).

To improve cycle stability, we investigated the effects of the fluoroethylene carbonate (FEC) electrolyte additive on the properties of the HCSi20 electrode. Figure 5b shows charging and discharging potential profile over 60 cycles, which shows 40–50% of the initial capacity after 60 cycles, which is significantly better than the stability in the cell with electrolyte without FEC, which drops to 20% after 10 cycles (Figure 5a).

During the galvanostatic procedures shown in Figure 4, impedance changes (GEIS) were measured in situ as a function of time. The resulting impedance spectra are shown in Figures 6–8.

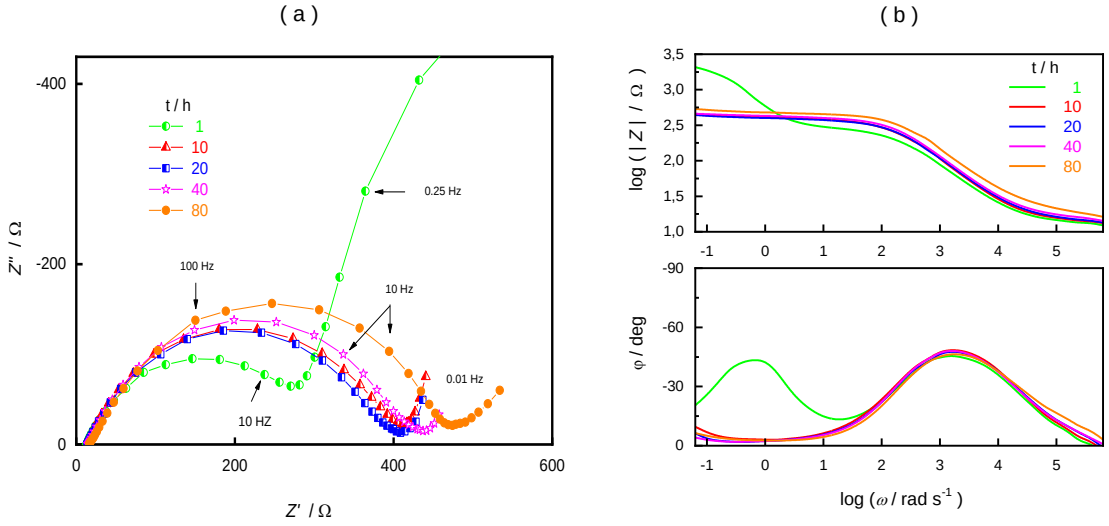

Figure 6. In situ GEIS impedance spectra for HCSi20 electrode in (**a**) Nyquist plot, (**b**) Bode plot.

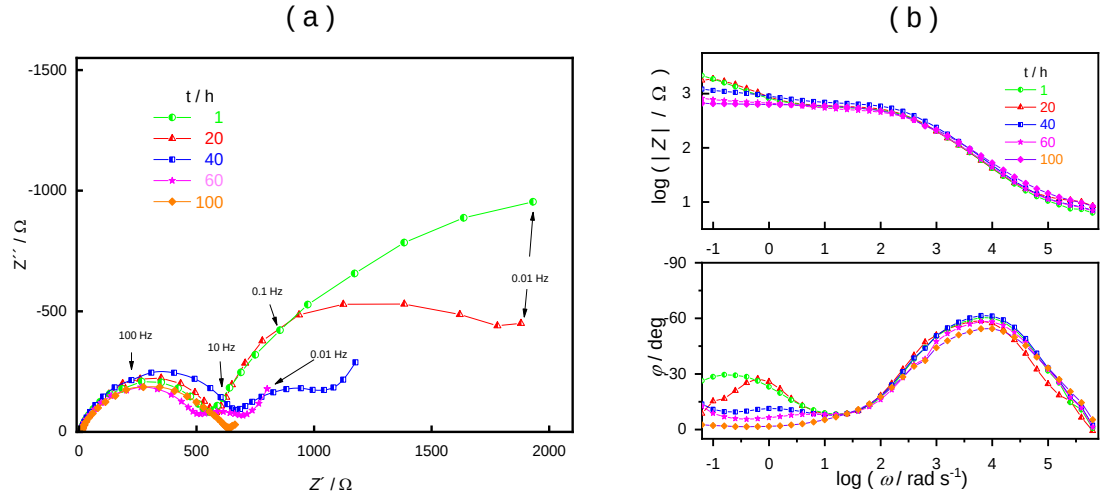

Figure 7. In situ GEIS impedance spectra for HCSi40 electrode in (**a**) Nyquist plot, (**b**) Bode plot.

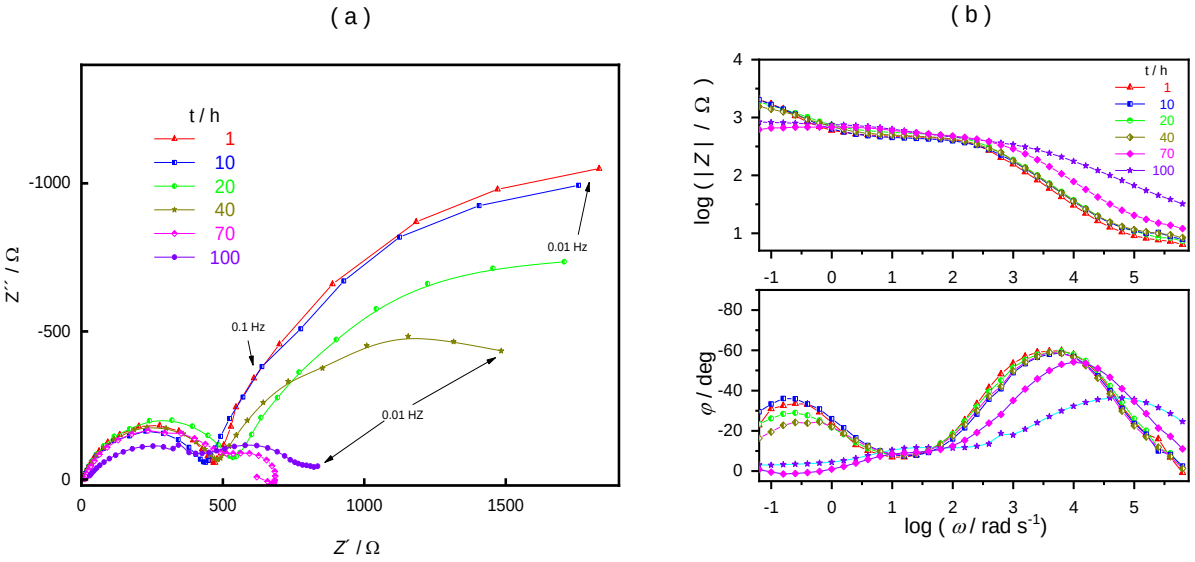

Figure 8. In situ GEIS impedance spectra for HCSi60 electrode in (**a**) Nyquist plot, (**b**) Bode plot.

From the dependencies shown, it is evident that only the impedance spectrum measured after one hour shows a low-frequency (LF) semicircuit connected with an additional series of parallel R || C combination. This impedance spectrum was measured at a potential of ≈+2.5 V, as shown by the chronopotentiometry curve in Figure 4, when the primary SEI is formed. As a result, the formation of SEI may be associated with the formation of an LF semicircuit; however, the impedance spectra measured at other refute this assumption. This LF semicircuit disappears in the other impedance spectra, so it is impossible to associate the formation of the primary SEI with the existence of this LF semicircuit. Since the conditions for the intercalation process are not met at this potential, the layer acts as a resistor. A semicircle associated with the charge transfer resistance (R_{ct}) on and within the electrode was registered in the other impedance spectra from 10 to 80 h. The intercalated Li^+ makes the layer more conductive, resulting in the loss of the semicircular dependence in the LF region registered in the first measurement.

The time-dependance GEIS impedance spectra for HCSi40 are shown on Figure 7. The presence of the LF semicircles is evident up to 60 h of the galvanostatic process, with resistances higher than the resistance registered for the HCSi20. Despite the intercalation of Li^+ ions registered up to 60 h (Figure 4), Li^+ has a harder time penetrating into the bulk due to the increased thickness of the layer, so that the resistive component of the layer is present for a longer time. The semicircle disappears after 60 h.

Figure 8 shows the time dependent GEIS impedance spectra for the thickest layer HCSi60. The presence of an LF semicircle throughout the galvanostatic process indicates that the resistive component dominates all the time. There is hard intercalation of Li^+ ions into the bulk and cannot eliminate the resistive component of the layer. Intercalation occurs in a single process (Figure 4) that changes only after 60 h, but the Li^+ ions continue to have difficulty penetrating deeper into the electrode.

By comparing in situ GEIS impedance spectra for all three thicknesses after 20 h of lithiation (Figure 9), we can conclude that, despite having the same capacities (≈3500 mAh g^{-1}), the thinnest electrode, HCSi20, allows diffusion of Li^+ ions into the bulk, while thicker layers prevent smooth diffusion into the bulk of the silicon electrode due to the increased resistance of the layer as shown on Figure 9.

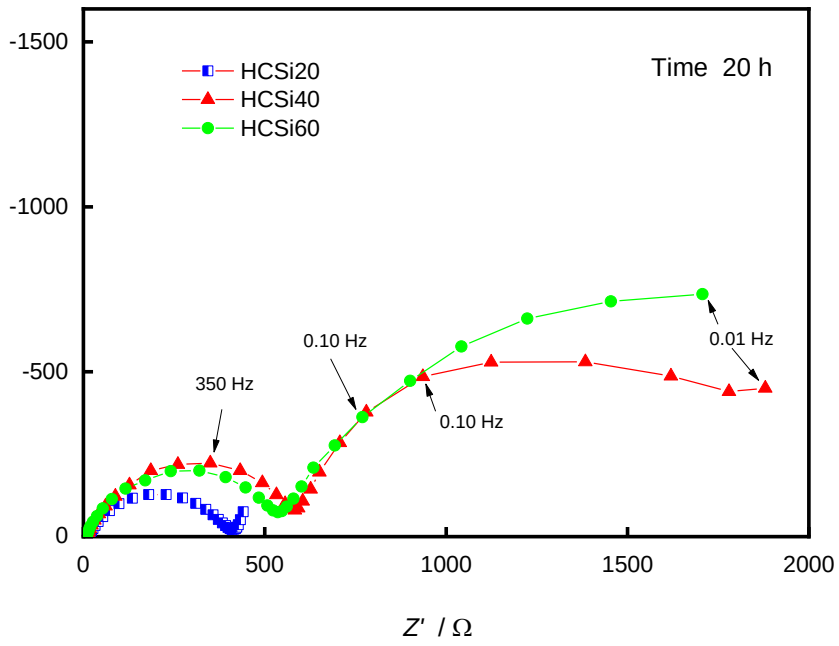

Figure 9. In situ GEIS impedance spectra compared for all three thicknesses after 20 h of lithiation in Nyquist plot.

Figure 10 compares in situ GEIS impedance spectra with FEC for all three thicknesses in Nyquist plot. The impedance is evidently lowest for the electrode HCSi20, confirming the easier lithiation. Furthermore, the addition of FEC reduces R_{ct} values significantly, confirming our assumptions. With the addition of FEC, the charge transfer resistance for HCSi20, which is ≈450 Ω, is reduced by nearly 4 times. Resistance values for thicker electrodes are slightly higher than 500 Ω, but with the addition of FEC, it drops to 200 Ω for the HCSi40 and 320 Ω for the HCSi60 electrode.

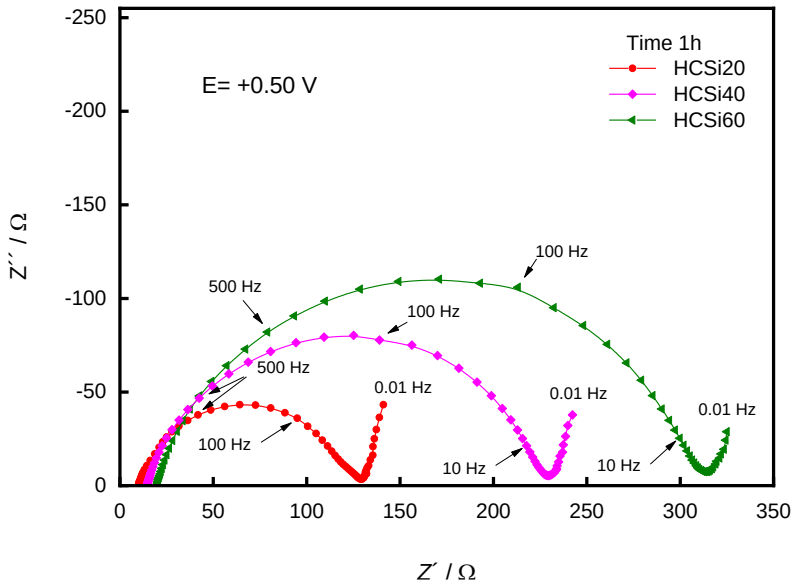

Figure 10. In situ GEIS impedance spectra compared for all three thicknesses with FEC in Nyquist plot.

Since a two-electrode system was used with Li metal as the counter electrode (CE), the contribution of Li to the total impedance must be considered [31–34]. In general, a total impedance of 2-electrode cell (Li-electrode, electrolyte, separator, HCSi-electrode) corresponds to the sum of the electrolyte resistance R_s, the resistance within the separator R_{sep}, the counter electrode impedance (Li-electrode), Z_{CE}, and the impedance of the working electrode (HCSi), Z_{WE}. In the high-frequency (HF) region, R_s and R_{sep} predominate and can be easily separated from the total impedance. Estimating contribution of the Z_{WE} and the Z_{CE} impedance requires additional measurements. Therefore, measurements of the Li impedance in a symmetric cell (Li-electrolyte-separator-Li) with an OCP of 0.0 V were performed.

The impedance spectrum of a symmetric cell (Li-Li) at OCP 0.0 V and an asymmetric cell (Li-HCSi20) at OCP +3.5 V are shown in Figure 11. The total impedance of the asymmetric cell is equal to the sum of the impedances Z_{Li}, as Z_{CE}, and Z_{HCSi}, as Z_{WE}, with the standard sum of electrolyte and separator resistance:

$$\text{Symmetric cell: } Ztot = 2ZLi + Rsep + Rs$$

$$\text{Asymmetric cell: } Ztot = ZLi + ZHCSi + Rsep + Rs$$

Since both impedance spectra were measured under OCP conditions, without additional polarization, we assume that the in the Z_{Li} in symmetric and asymmetric cell is equal, since Li is in same equilibrium with the electrolyte used in both cases. Under this assumption, subtracting the Z_{Li} measured in the symmetric cell which represents the Z_{CE}, from the total impedance of the asymmetric cell, we obtain the impedance of the working electrode (HCSi20), also shown in Figure 11.

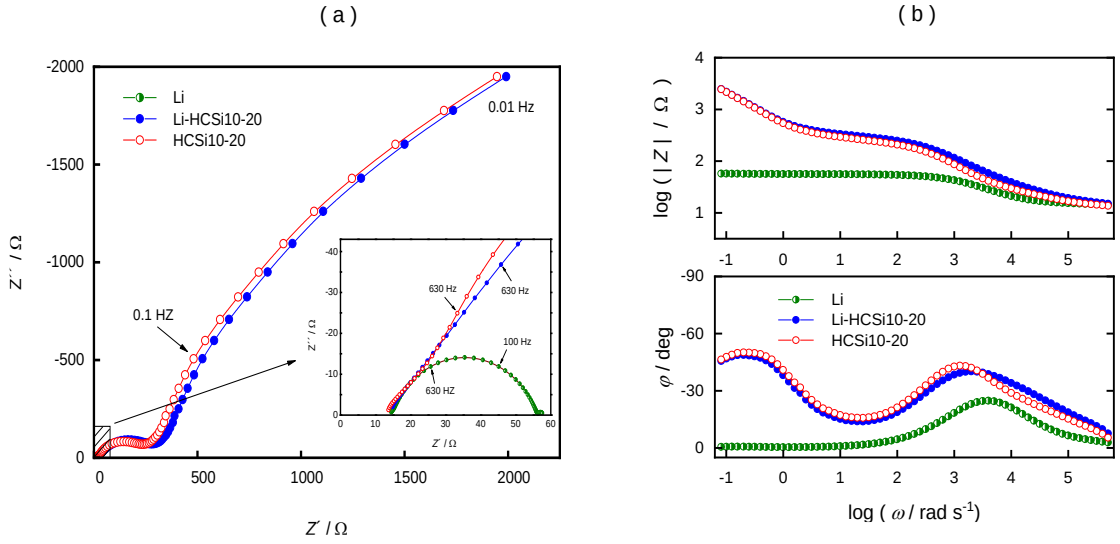

Figure 11. Impedance spectra of symmetric cell (Li-Li) at OCP 0.0 V and asymmetric cell. (Li-HCSi20) at OCP +3.5 V in (**a**) Nyquist plot, (**b**) Bode plot.

In this case, the impedance was measured as a function of time at constant current flowing through the cell simultaneously with an AC bias GEIS signal. At constant current density, we can assume that oxidation of Li is constant, with constant impedance at the CE, so that any change in the measured impedance of the asymmetric cell corresponds to a change in the Z_{WE}. Galvanostatic measurements are also performed in a 2-electrode combination, allowing measurements to be more reliably correlated with galvanostatic measurements.

Figure 12 shows the impedance spectra of HCSi20 cell polarized at E = +0.05 V. In the frequency range up to 0.5 Hz, all spectra show a semicircular dependence. The resistance to charge transfer is related to the intercalation of Li^+ ions, but this process is complex and not uniquely related to a single reaction, as is the case with a redox reaction in a solution.

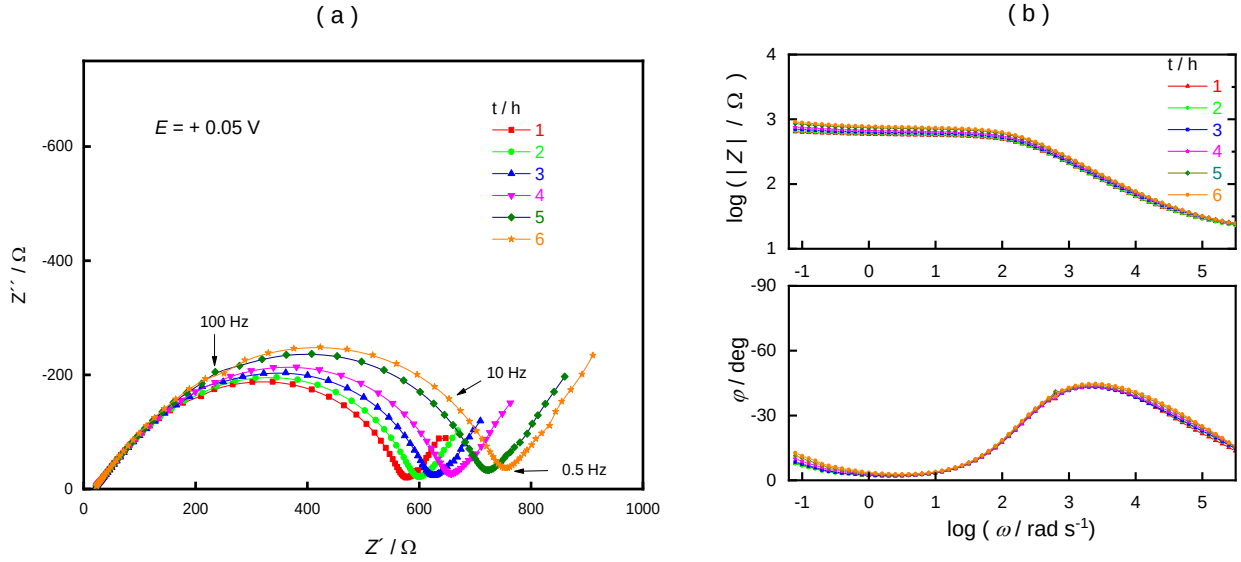

Figure 12. Time-dependance PEIS spectra of HCSi20 cell at +0.05 V in (**a**) Nyquist plot, (**b**) Bode plot.

A HF semicircular dependence (Figure 12) associated with the R_{ct} shows significant asymmetry connected only with the mechanism of intercalation of Li^+ ions, which is not the case at Figure 13 where R_{ct} is significantly smaller, and asymmetry is absent.

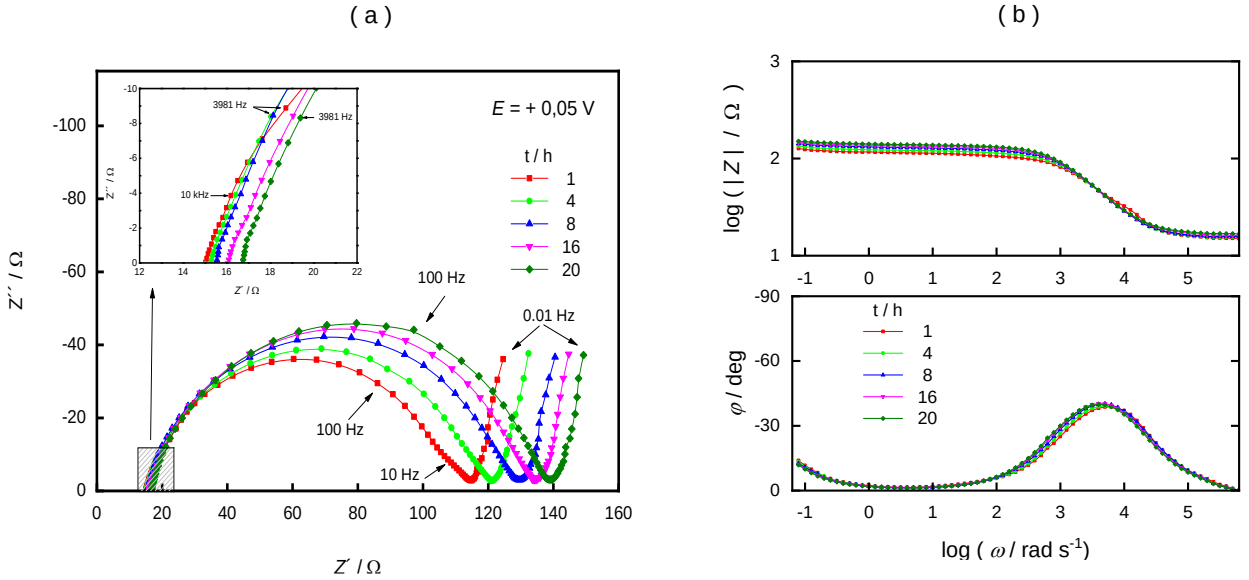

Figure 13. Time-dependance PEIS spectra of HCSi20 with FEC cell at +0.05 V in (**a**) Nyquist plot, (**b**) Bode plot.

In the HF region (Figure 13 inset), the resistance connected with the resistance of the electrolyte between the electrodes and the resistance of the separator, slightly increases with time. The increase in resistance could be attributed to a change in electrolyte composition and the gradual formation of the SEI layer. Since there is no semicircular dependence anomaly in the impedance displays in Figure 13, we assume that its influence could manifest as an increase in resistance due to the layer's electrical properties.

Because the dynamics of SEI layer formation varies, charge transfer resistance values are likely lower with the addition of FEC. As shown in the Figure 14, R_{ct} increases slightly, but with the addition of FEC, this value is stabilized over long periods of lithiation (>20 h).

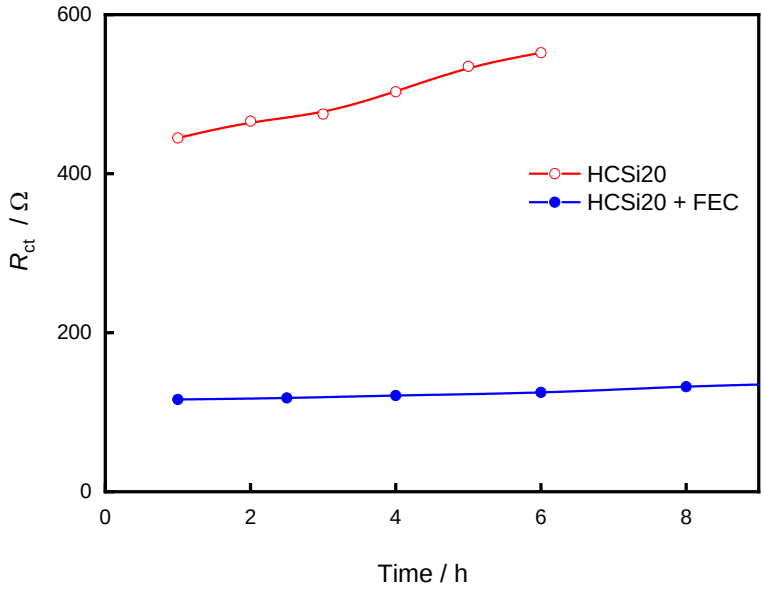

Figure 14. Charge transfer resistance (R_{ct}) change over long period of lithiation for electrode HCSi20 and HCSi20 with the addition of FEC.

In the research of materials for Li-ion cells, when the intercalation of Li^+ ions in the structure of the Si-electrode is present, there are processes that take place in a series, one after the other: (a) diffusion of Li^+ ions through the electrolyte and separator to the

surface of the Si-electrode, (b) migration of Li^+ ions through the surface film, (c) charge transfer reactions, (d) diffusion through the solid phase of the electrode and, finally, (e) ion accumulation manifested as a capacity. In any case, all these processes affect the total impedance, so the model that describes the impedance spectrum should include the effects of these processes in series. The so-called Voigt model, which faithfully describes the influence of certain processes and consists of several serial R ‖ C parallel combinations, is frequently used [20,35,36]. The anomaly of the HF semicircular dependence can be explained using such a model.

Figure 15a shows a typical impedance spectrum of the Si-electrode in the Nyquist plot, with a pronounced anomaly of the semicircular dependence, visible also in the dependence of the phase angle (Bode plot).

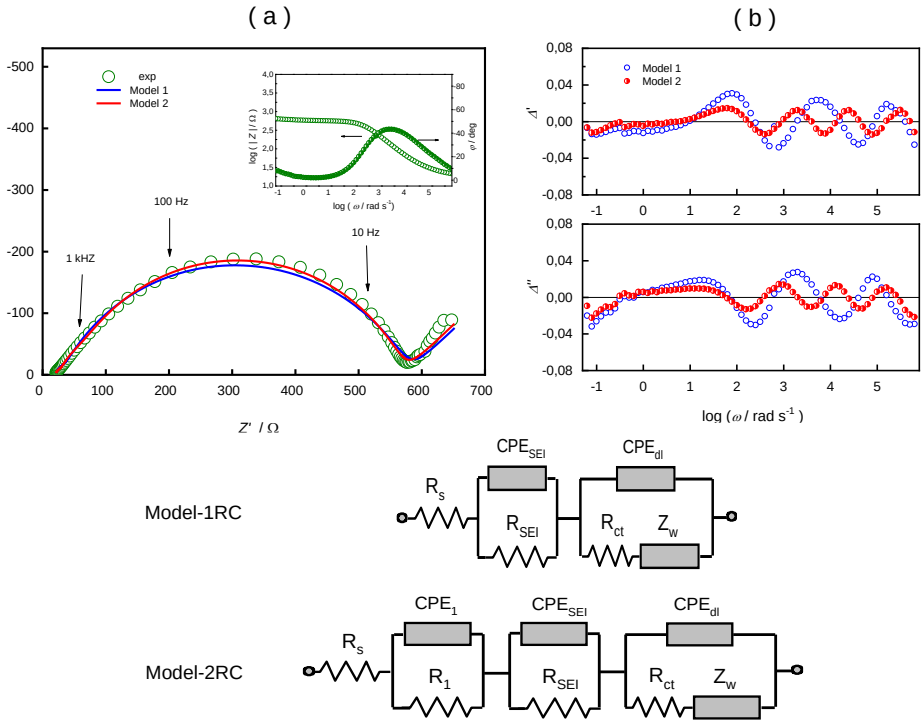

Figure 15. Time-dependance PEIS spectra of HCSi20 cell at +0.05 V in (**a**) Nyquist plot, (**b**) residuals.

The Voigt model was used to analyze the frequency dependence, in which the classic Randles circuit is connected in series with one or two R ‖ C parallel combinations. Figure 15b shows the model's adaptation quality to the measured frequency dependence of the cell as residuals, deviations of the real and imaginary components between the measured values and the values obtained by applying models 1 and 2. We can conclude from the obtained dependences, that model 2 provides a satisfactory fit of the frequency dependence, where two R ‖ C parallel circuits represent processes that have a direct impact on the semicircular dependency anomaly. One R ‖ C circuit could be connected to the formation of the SEI, while the other R ‖ C circuit could be a contribution of the Li-electrode, because the measurement was performed in a so-called two-electrode combination.

These studies compare three electrode thicknesses side by side, with the thinnest one regarded as the most optimal. We demonstrated the addition of electrolyte additive, FEC, increased the number of cycles. These studies have the potential to make a significant contribution to silicon anode material optimization.

4. Conclusions

We demonstrated the significance of electrode thickness in anode design in this paper. We concluded that the intercalation of Li^+ ions into the thicker electrodes is difficult by systematically comparing three different electrode thicknesses (20, 40 and 60 µm). One

of the causes could be increased resistance as layer thickness increases. Despite having the same capacities (≈3500 mAh g^{-1}), the thickest electrode, HCSi20, allows diffusion of Li^+ ions into the bulk, whereas thicker layers prevent smooth diffusion into the bulk of the silicon electrode due to increased layer resistance. To increase the number of charge and discharge cycles, we improved the electrolyte by adding fluoroethylene carbonate (FEC), which reduced the capacity of HCSi20 electrode to 50% of the initial capacity (≈3500 mAh g^{-1}) after 60 cycles, whereas it dropped to 20% of the initial capacity after 10 cycles without the addition of FEC. The charge transfer resistance for HCSi20, which is 450, is nearly four times reduced with the addition of FEC. Resistance values for thicker electrodes are slightly higher than 500, but with FEC, they drop to 200 for the HCSi40 electrode and 320 for the HCSi60 electrode. These results can greatly contribute to the further optimization of the anode materials.

Author Contributions: Conceptualization, M.R. and K.K.; Formal analysis, M.R.; Funding acquisition, M.I.; Investigation, M.R., K.K.; Methodology, M.R., K.K., N.B.; Project administration, M.I.; Resources, M.I.; Supervision, K.K., M.I.; Visualization, M.R.; Writing—original draft, M.R.; Writing—review & editing, M.R., K.K., L.M. and M.I. All authors have read and agreed to the published version of the manuscript.

Funding: This work has been fully supported by the Competitiveness and Cohesion Operational Programme, a project co-financed by the Croatian Government and the European Union through the European Regional Development Fund (KK.01.1.1.01.0001).

Data Availability Statement: Not applicable.

Conflicts of Interest: The authors declare no conflict of interest.

References

1. Ashuri, M.; He, Q.; Shaw, L.L. Silicon as a Potential Anode Material for Li-Ion Batteries: Where Size, Geometry and Structure Matter. *Nanoscale* **2016**, *8*, 74–103. [CrossRef] [PubMed]
2. Salah, M.; Murphy, P.; Hall, C.; Francis, C.; Kerr, R.; Fabretto, M. Pure Silicon Thin-Film Anodes for Lithium-Ion Batteries: A Review. *J. Power Sources* **2019**, *414*, 48–67. [CrossRef]
3. Raić, M.; Mikac, L.; Marić, I.; Štefanić, G.; Škrabić, M.; Gotić, M.; Ivanda, M. Nanostructured Silicon as Potential Anode Material for Li-Ion Batteries. *Molecules* **2020**, *25*, 891. [CrossRef] [PubMed]
4. Wei, Q.; Liu, G.C.; Zhang, C.; Hong, X.J.; Song, C.L.; Yang, Y.; Zhang, M.; Huang, W.; Cai, Y.P. Novel Honeycomb Silicon Wrapped in Reduced Graphene Oxide/CNT System as High-Stability Anodes for Lithium-Ion Batteries. *Electrochim. Acta* **2019**, *317*, 583–593. [CrossRef]
5. Li, P.; Zhao, G.; Zheng, X.; Xu, X.; Yao, C.; Sun, W.; Dou, S.X. Recent Progress on Silicon-Based Anode Materials for Practical Lithium-Ion Battery Applications. *Energy Storage Mater.* **2018**, *15*, 422–446. [CrossRef]
6. Devaux, D.; Leduc, H.; Dumaz, P.; Lecuyer, M.; Deschamps, M.; Bouchet, R. Effect of Electrode and Electrolyte Thicknesses on All-Solid-State Battery Performance Analyzed With the Sand Equation. *Front. Energy Res.* **2020**, *7*, 168. [CrossRef]
7. Eshetu, G.G.; Zhang, H.; Judez, X.; Adenusi, H.; Armand, M.; Passerini, S.; Figgemeier, E. Production of High-Energy Li-Ion Batteries Comprising Silicon-Containing Anodes and Insertion-Type Cathodes. *Nat. Commun.* **2021**, *12*, 5459. [CrossRef]
8. Singh, M.; Kaiser, J.; Hahn, H. Thick Electrodes for High Energy Lithium Ion Batteries. *J. Electrochem. Soc.* **2015**, *162*, A1196–A1201. [CrossRef]
9. Bo, Z.; Cheng, X.; Yang, H.; Guo, X.; Yan, J.; Cen, K.; Han, Z.; Dai, L. Ultrathick MoS_2 Films with Exceptionally High Volumetric Capacitance. *Adv. Energy Mater.* **2022**, *12*, 2103394. [CrossRef]
10. Bo, Z.; Yi, K.; Yang, H.; Guo, X.; Huang, Z.; Zheng, Z.; Yan, J.; Cen, K.; Ostrikov, K. More from Less but Precise: Industry-Relevant Pseudocapacitance by Atomically-Precise Mass-Loading MnO_2 within Multifunctional MXene Aerogel. *J. Power Sources* **2021**, *492*, 229639. [CrossRef]
11. Zheng, H.; Li, J.; Song, X.; Liu, G.; Battaglia, V.S. A Comprehensive Understanding of Electrode Thickness Effects on the Electrochemical Performances of Li-Ion Battery Cathodes. *Electrochim. Acta* **2012**, *71*, 258–265. [CrossRef]
12. Zhao, R.; Liu, J.; Gu, J. The Effects of Electrode Thickness on the Electrochemical and Thermal Characteristics of Lithium Ion Battery. *Appl. Energy* **2015**, *139*, 220–229. [CrossRef]
13. Bisquert, J. Influence of the boundaries in the impedance of porous film electrodes. *Phys. Chem. Chem. Phys.* **2000**, *2*, 4185–4192. [CrossRef]
14. Umeda, M.; Dokko, K.; Fujita, Y.; Mohamedi, M.; Uchida, I.; Selman, J.R. Electrochemical Impedance Study of Li-Ion Insertion into Mesocarbon Microbead Single Particle Electrode: Part I. Graphitized Carbon. *Electrochim. Acta* **2001**, *47*, 885–890. [CrossRef]

15. Levi, M.D.; Levi, E.A.; Aurbach, D. The Mechanism of Lithium Intercalation in Graphite Film Electrodes in Aprotic Media. Part 2. Potentiostatic Intermittent Titration and in Situ XRD Studies of the Solid-State Ionic Diffusion. *J. Electroanal. Chem.* **1997**, *421*, 89–97. [CrossRef]
16. Levi, M.D.; Aurbach, D. The Mechanism of Lithium Intercalation in Graphite Film Electrodes in Aprotic Media. Part 1. High Resolution Slow Scan Rate Cyclic Voltammetric Studies and Modeling. *J. Electroanal. Chem.* **1997**, *421*, 79–88. [CrossRef]
17. Zhu, P.; Slater, P.R.; Kendrick, E. Insights into Architecture, Design and Manufacture of Electrodes for Lithium-Ion Batteries. *Mater. Des.* **2022**, *223*, 111208. [CrossRef]
18. Ogihara, N.; Itou, Y.; Sasaki, T.; Takeuchi, Y. Impedance Spectroscopy Characterization of Porous Electrodes under Different Electrode Thickness Using a Symmetric Cell for High-Performance Lithium-Ion Batteries. *J. Phys. Chem. C* **2015**, *119*, 4612–4619. [CrossRef]
19. Raić, M.; Mikac, L.; Gotić, M.; Škrabić, M.; Baran, N.; Ivanda, M. Ag Decorated Porous Si Structure as Potential High-Capacity Anode Material for Li-Ion Cells. *J. Electroanal. Chem.* **2022**, *922*, 116743. [CrossRef]
20. Aurbach, D.; Zaban, A. Impedance Spectroscopy of Lithium Electrodes. Part 1. General Behavior in Propylene Carbonate Solutions and the Correlation to Surface Chemistry and Cycling Efficiency. *J. Electroanal. Chem.* **1993**, *348*, 155–179. [CrossRef]
21. Bordes, A.; Eom, K.S.; Fuller, T.F. The Effect of Fluoroethylene Carbonate Additive Content on the Formation of the Solid-Electrolyte Interphase and Capacity Fade of Li-Ion Full-Cell Employing Nano Si-Graphene Composite Anodes. *J. Power Sources* **2014**, *257*, 163–169. [CrossRef]
22. Xu, C.; Lindgren, F.; Philippe, B.; Gorgoi, M.; Björefors, F.; Edström, K.; Gustafsson, T. Improved Performance of the Silicon Anode for Li-Ion Batteries: Understanding the Surface Modification Mechanism of Fluoroethylene Carbonate as an Effective Electrolyte Additive. *Chem. Mater.* **2015**, *27*, 2591–2599. [CrossRef]
23. Etacheri, V.; Haik, O.; Goffer, Y.; Roberts, G.A.; Stefan, I.C.; Fasching, R.; Aurbach, D. Effect of Fluoroethylene Carbonate (FEC) on the Performance and Surface Chemistry of Si-Nanowire Li-Ion Battery Anodes. *Langmuir* **2012**, *28*, 965–976. [CrossRef] [PubMed]
24. Moškon, J.; Talian, S.D.; Dominko, R.; Gaberšček, M. Advances in Understanding Li Battery Mechanisms Using Impedance Spectroscopy. *J. Electrochem. Sci. Eng.* **2020**, *10*, 79–93. [CrossRef]
25. Raccichini, R.; Amores, M.; Hinds, G. Critical Review of the Use of Reference Electrodes in Li-Ion Batteries: A Diagnostic Perspective. *Batteries* **2019**, *5*, 12. [CrossRef]
26. Meddings, N.; Heinrich, M.; Overney, F.; Lee, J.S.; Ruiz, V.; Napolitano, E.; Seitz, S.; Hinds, G.; Raccichini, R.; Gaberšček, M.; et al. Application of Electrochemical Impedance Spectroscopy to Commercial Li-Ion Cells: A Review. *J. Power Sources* **2020**, *480*, 228742. [CrossRef]
27. Ko, Y.; Hwang, C.; Song, H.K. Investigation on Silicon Alloying Kinetics during Lithiation by Galvanostatic Impedance Spectroscopy. *J. Power Sources* **2016**, *315*, 145–151. [CrossRef]
28. Ji, X.; Nazar, L.F. Advances in Li-S Batteries. *J. Mater. Chem.* **2010**, *20*, 9821–9826. [CrossRef]
29. Zhou, X.; Li, P.; Tang, Z.; Liu, J.; Zhang, S.; Zhou, Y.; Tian, X. FEC Additive for Improved SEI Film and Electrochemical Performance of the Lithium Primary Battery. *Energies* **2021**, *14*, 7467. [CrossRef]
30. Schellenberger, M.; Golnak, R.; Quevedo Garzon, W.G.; Risse, S.; Seidel, R. Accessing the Solid Electrolyte Interphase on Silicon Anodes for Lithium-Ion Batteries in-Situ through Transmission Soft X-ray Absorption Spectroscopy. *Mater. Today Adv.* **2022**, *14*, 100215. [CrossRef]
31. Klink, S.; Höche, D.; La Mantia, F.; Schuhmann, W. FEM Modelling of a Coaxial Three-Electrode Test Cell for Electrochemical Impedance Spectroscopy in Lithium Ion Batteries. *J. Power Sources* **2013**, *240*, 273–280. [CrossRef]
32. Hoshi, Y.; Narita, Y.; Honda, K.; Ohtaki, T.; Shitanda, I.; Itagaki, M. Optimization of Reference Electrode Position in a Three-Electrode Cell for Impedance Measurements in Lithium-Ion Rechargeable Battery by Finite Element Method. *J. Power Sources* **2015**, *288*, 168–175. [CrossRef]
33. Costard, J.; Ender, M.; Weiss, M.; Ivers-Tiffée, E. Three-Electrode Setups for Lithium-Ion Batteries. *J. Electrochem. Soc.* **2017**, *164*, A80–A87. [CrossRef]
34. Baker, D.R.; Verbrugge, M.W.; Hou, X.X. A Simple Formula Describing Impedance Artifacts Due to the Size and Surface Resistance of a Reference-Electrode Wire in a Thin-Film Cell. *J. Electrochem. Soc.* **2017**, *164*, A407–A417. [CrossRef]
35. Thevenin, J.G.; Muller, R.H. Impedance of Lithium Electrodes in a Propylene Carbonate Electrolyte. *J. Electrochem. Soc.* **1987**, *134*, 273–280. [CrossRef]
36. Zaban, A.; Zinigrad, E.; Aurbach, D. Impedance Spectroscopy of Li Electrodes. 4. A General Simple Model of the Li-Solution Interphase in Polar Aprotic Systems. *J. Phys. Chem.* **1996**, *100*, 3089–3101. [CrossRef]

Disclaimer/Publisher's Note: The statements, opinions and data contained in all publications are solely those of the individual author(s) and contributor(s) and not of MDPI and/or the editor(s). MDPI and/or the editor(s) disclaim responsibility for any injury to people or property resulting from any ideas, methods, instructions or products referred to in the content.